Motional-Stark Effect (MSE)

Introduction

The *Stark Effect* is the shifting and splitting of the electronic energy levels due to an external electric field. The *Motional-Stark Effect (MSE)*, instead, is the specific case in which the electric field is the Lorentz electric field felt by an atom moving in a magnetic field $\mathbf{B}$ at a velocity $\mathbf{v}$, in its rest frame: $\mathbf{E} = \mathbf{v} \times \mathbf{B}$.

In plasma physics, the Motional-Stark Effect (MSE) serves as a crucial diagnostic tool for determining the poloidal magnetic field $\mathbf{B_P}$ within the plasma. Accurate knowledge of the poloidal magnetic field is essential for understanding plasma stability and the formation of Internal Transport Barriers (ITBs). Additionally, MSE measurements enable inference of the plasma current distribution, since the current density $\mathbf{J}$ is related to the magnetic field $\mathbf{B}$ through Ampère's law:

$$\nabla \times \mathbf{B} = \mu_0 \mathbf{J}.$$

In TCV, the poloidal magnetic field is determined by the LIUQE (from "EQUIL" spelt backwards) code, which is an equilibrium code based on the resolution of the Grad-Shafranov equation, and on magnetic probes measurements outside of the plasma. However, when using Neutral Beam Heating (NBH) and Electron Cyclotron Resonance Heating (ECRH), the plasma equilibrium velocity is not negligible anymore, and the magnetic field is locally influenced. This explains the need for the Motional-Stark Effect diagnostic, which provides a direct measurement of the local magnetic field inside the plasma, unaffected by external equilibrium assumptions.

A bit of history

The Stark effect was discovered by the German physicist Johannes Stark in 1913, for which he was awarded the nobel price in 1919. During the same year the effect was independently discovered by the Italian physicit Antonio Lo Surdo[1].

Physical principles

The MSE diagnostic is based on the external injection of neutral beam deuterium atoms and, when entering the plasma, they are subject to inelastic collisions with plasma's ions and electrons. The neutrals' electrons, which initially are in their ground state, can reach a higher energy level, E_2 and, when they decay to a lower energy state E_1, they emit a photon with energy $E_\gamma = E_2 - E_1$, and wavelength $\lambda = \frac{hc}{E_\gamma}$.

In particular, of specific interest is the Balmer-α emission of the deuterium atom D_α, which corresponds to the transition between $n = 3$ and $n = 2$, and is characterized by an energy $E_{D_\alpha} = 1.89$ eV and a wavelength $\lambda_{D_\alpha} = 656.279$ nm. This is because the D_α emission has a high emission intensity in the visible spectrum (red light), and it is highly Doppler-shifted with respect to the plasma D_α emission. Moreover, since the neutral's velocity across the magnetic field is high compared to the thermal velocity of the plasma ions, the resulting Lorentz electric field $\mathbf{E_L} = \mathbf{v} \times \mathbf{B}$ is significant. This leads to a measurable splitting and polarization of the D_α, spectral line, which can be used to infer the local magnetic field direction and magnitude inside the plasma.

To analyze the Stark effect in the deuterium atom, it is convenient to solve the non-relativistic Schrödinger Equation using parabolic coordinates. In this framework, the atomic states are described by four quantum numbers $|n, n_1, n_2, m\rangle$: n is the principal quantum number, n_1 and n_2 are parabolic quantum numbers, and m is the magnetic quantum number. The energy splitting caused by the Stark effect, calculated using first-order perturbation theory, is given by[2]:

$$\Delta E^{(1)} = \frac{3}{2} e a_0 n (n_1 - n_2) |\mathbf{E_L}|,$$

where e is the elementary charge, and a_0 is the Bohr radius.

In Figure 1 the lines splitting of the energy levels with principal quantum numbers $n = 2$ and $n = 3$ is shown. For clarity the fine structure splitting is not shown.

The separation of the spectral lines, as shown in Figure 2, is directly proportional to the strength of the electric field[3]:

$$\Delta\lambda \approx \frac{3 e a_0 |\mathbf{E_L}| \lambda_0^2}{2hc},$$

where λ_0 is the unshifted Balmer-α wavelength, h is Planck's constant, and c is the speed of light.

The and components are resepectively polarized parallel and perpendicular to the electric field. This means that when trying to catch the radiation, the instensity of the components

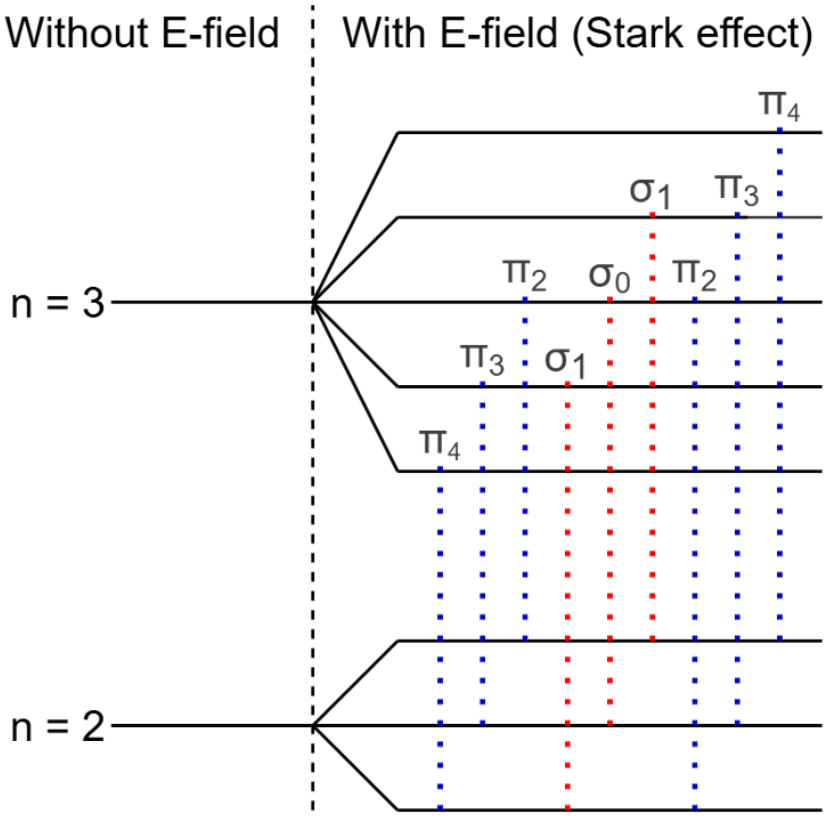

Figure 1: D_α splitting due to MSE[3].

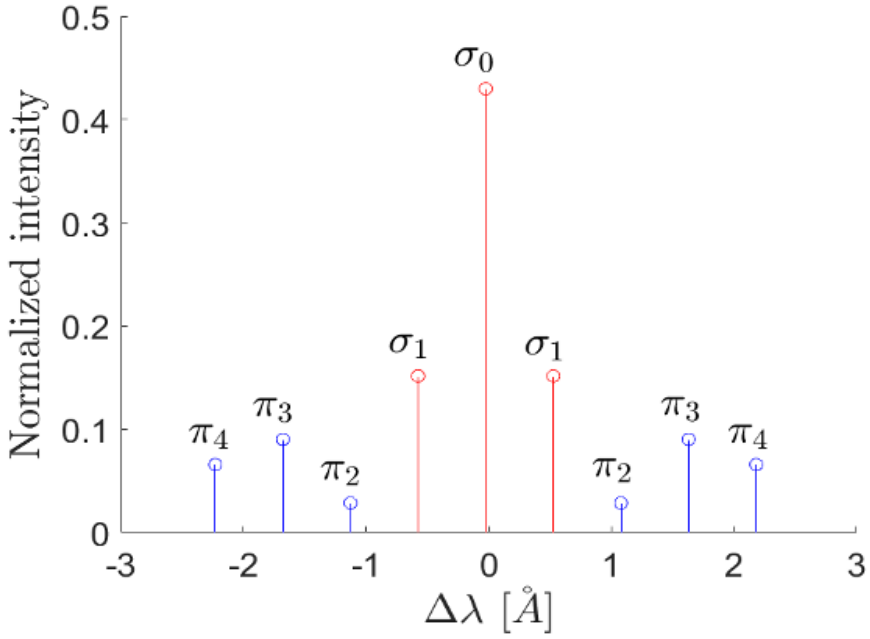

Figure 2: Spectral lines separation of the D_α radiation due to MSE[3].

depend on the direction of the line-of-sight (LOS) respect to $\mathbf{E_L}$. Defining with Ψ the angle between the LOS and $\mathbf{E_L}$, the observed intensities scale as:

$$I_\sigma \propto 1 + \cos^2 \Psi,$$

$$I_\pi \propto \sin^2 \Psi.$$

MSE diagnostic on TCV

The MSE diagnostic on TCV relies on the deuterium neutrals injected by the NBI-1 of TCV. Along the beam 20 LOS are defined, originating from the optical setup at the bottom of TCV, as shown in Figure **??**.

To detect the Doppler-shifted radiation emitted by the neutral beam, each line-of-sight (LOS) must be oriented at an angle other than 90° relative to the beam direction. This arrangement ensures that the neutral beam has a velocity component along the LOS, making the Doppler-shifted emission distinguishable from the background plasma radiation.

As shown in Figure 4, the D spectrum exhibits several distinct peaks:

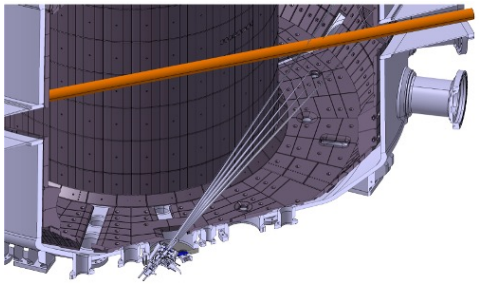

(a) Intersection of LOS (in grey) with the NBI (in orange)[3].

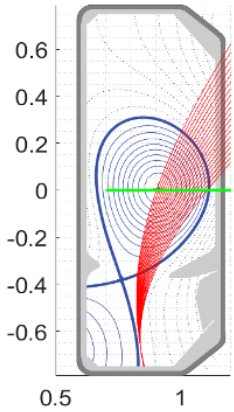

(b) Poloidal cross section of TCV with an example of magnetic equilibrium. In red the LOS and in green the NBI[3].

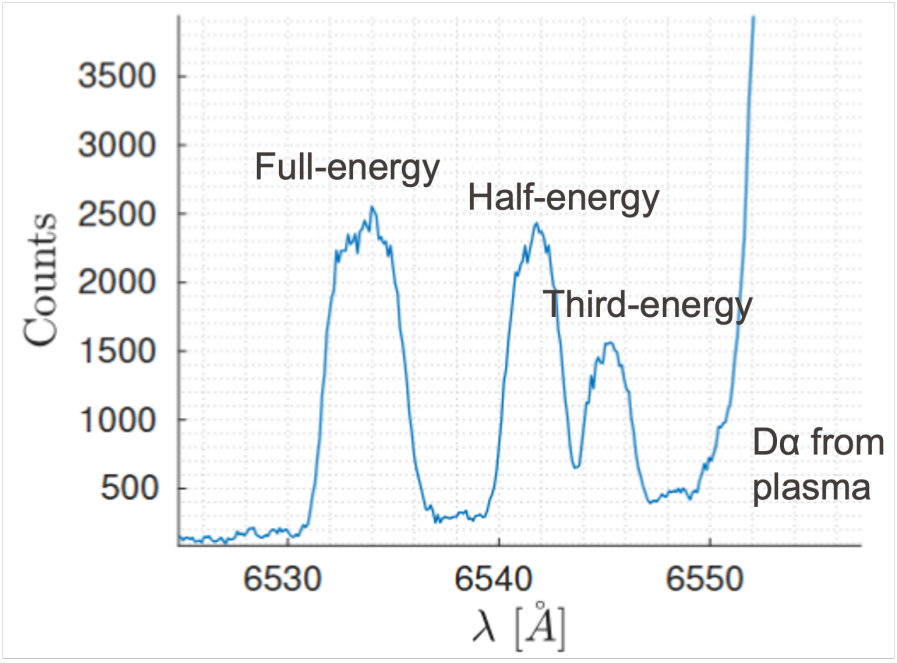

Figure 4: D radiation

- The full-energy peak corresponds to emission from D^+ ions;
- The half-energy peak arises from D_2^+ ions;
- The third-energy peak is due to D_3^+ ions;
- The remaining portion of the spectrum is non-shifted radiation emitted by the plasma.

These energy shifts result from the different velocities of the ion species, which are determined by their respective masses.

Table 1: Parameters of each LOS. R_{inter} is the radial position of the intersection between LOS and NBI-1, is the angle between LOS and NBI-1, is the doppler shift, and R is the radial resolution[3].

LOS	R_{inter} [m]	[deg]	Doppler shift [Å]	resolution R [cm ^{1}]
1	1.1062	138.61	-27.1349	6.4
2	1.0920	138.04	-26.8964	6.5
3	1.0783	137.48	-26.6568	6.4
4	1.0651	136.91	-26.4158	6.1
5	1.0524	136.35	-26.1734	5.8
6	1.0402	135.80	-25.9294	5.6
7	1.0278	135.24	-25.6837	5.5
8	1.0163	134.69	-25.4361	5.2
9	1.0053	134.13	-25.1867	5.0
10	0.9952	133.58	-24.9351	4.8
11	0.9849	133.03	-24.6813	4.6
12	0.9748	132.48	-24.4251	4.4
13	0.9651	131.92	-24.1664	4.2
14	0.9556	131.37	-23.9049	4.1
15	0.9464	130.81	-23.6407	3.9
16	0.9374	130.26	-23.3733	3.7
17	0.9283	129.70	-23.1028	3.5
18	0.9198	129.14	-22.8288	3.4
19	0.9116	128.57	-22.5512	3.2
20	0.9035	128.00	-22.2697	3.0

In Table 1 all the parameters relative to the intersection between the LOSs and the NBI-1 are listed.

The optical setup, shown in Figure 5, is composed by:

- A *beamsplitter plate* used to separate two orthogonal light polarizations of the D_α emission into two different barches. This is done because only the Motional Stark and the Zeeman effects actually influence the line polarization. A thin plate has been chosen to minimize

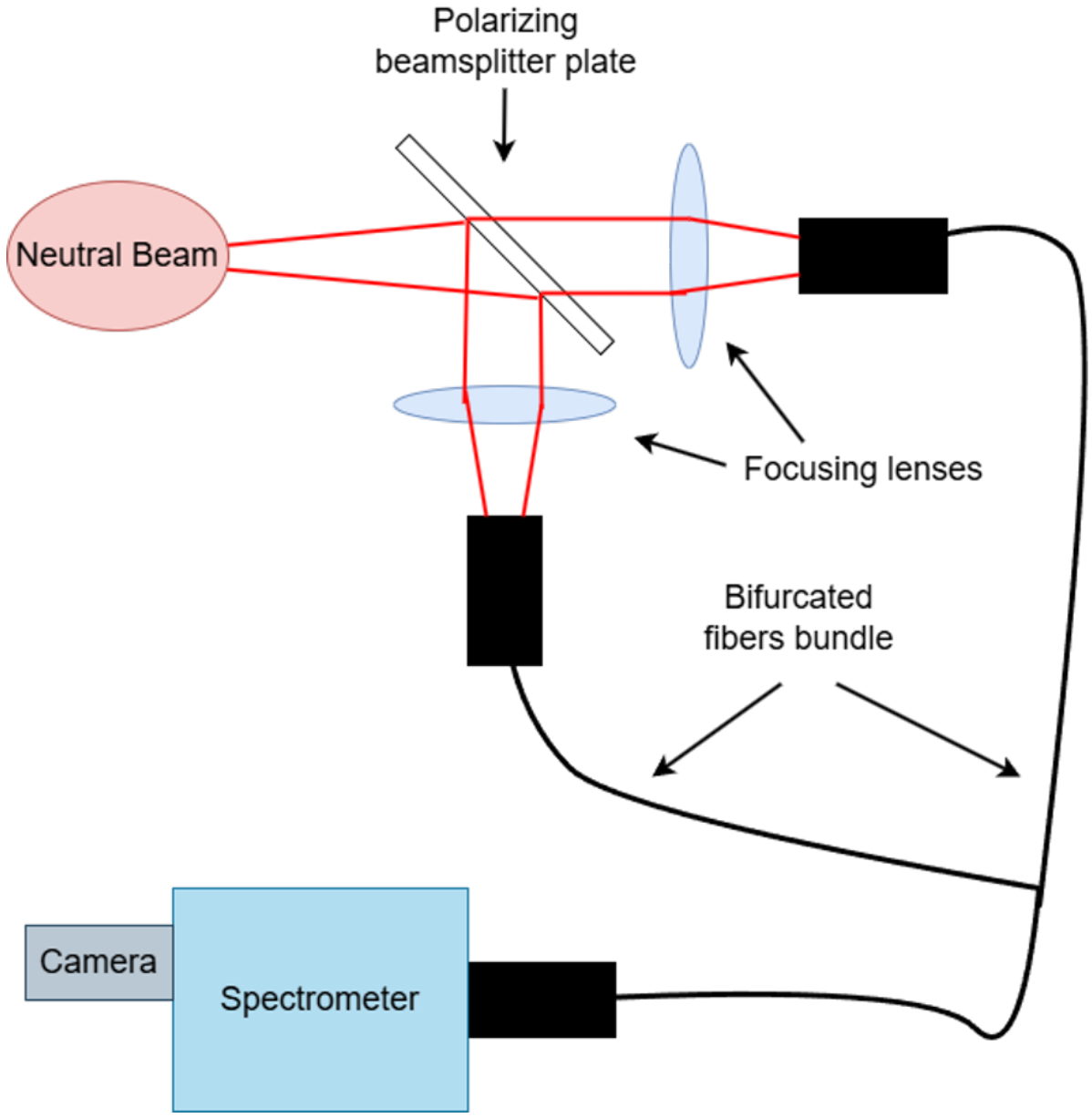

Figure 5: Optical setup of the MSE diagnostic[3]

the rotation β of the light polarization due to the Faraday effect. Currently, taking into account the 5 mm diagnostic window and the beamsplitter plate, the total rotation is

$$\beta = \beta_{\mathrm{w}} + \beta_{\mathrm{p}} \approx 1.2^{\circ} + 0.3^{\circ} = 1.5^{\circ}.$$

- 2 *lents*, one for each branch, used to focus the light into the optical fibers.
- 40 *optical fibers*, 20 per branch, which transmit the light to the spectrometer and the camera.

More details regarding the optical setup are listed in Table 2.

Table 2: Parameters of the optical components[3].

Parameter	**Spectrometer**	**Camera**	**Fibers**
Focal length	500 mm		
F#	4		
Grating	2400 grooves/mm		
Resolution	~ 0.5 Å		
Range	3800-8000 Å		
Model		Andor EMCCD	
Pixel size		13 µm	
Array size		1024x1024	
Time resolution		20 ms	
Camera range		3800-9000 Å	
Length of each fiber			30 m
Core diameter			295 µm
#fibers per branch			20
#branches			2
Fiber range			3800-8500 Å

References

1. Wikipedia. Stark effect.
2. Anh-Tai, T. D., Khang, L. M., Vy, N. D., Truong, T. D. H. & Pham, V. N. T. A revisit on the hydrogen atom induced by a uniform static electric field. (2024).
3. Müller, S. Implementation of polarization-resolved motional-stark spectroscopy on TCV. (École Polytechnique Fédérale de Lausanne (EPFL), 2025).